Fabrication of Protein-Conjugated Silver Sulfide Nanorods in the Bovine Serum Albumin Solution

Lin Yang,*,† Ruimin Xing,*,† Qingming Shen,† Kai Jiang,† Feng Ye,† Jinye Wang,‡ and Qiushi Ren*,§

College of Chemistry and Environmental Science, Henan Normal University, Xinxiang 453007, P. R. China, Biomedical Engineering, Shanghai Jiao Tong University, Shanghai 200030, P. R. China, and Institute for Laser Medicine and Bio-Photonics, Shanghai Jiao Tong University, Shanghai 200030, P. R. China

Received: October 1, 2005; In Final Form: March 14, 2006

Highly ordered silver sulfide nanorods conjugated with the Bovine Serum Albumin (BSA) protein have been successfully achieved at ambient temperature. Such a process is very simple and controllable, directly using silver nitrate and thioacetamide (TAA) as the reactants in the aqueous solution of BSA. The products have been characterized by XRD, HRTEM-SAED, SEM-EDS, TG-DTA, FT-IR, and CD spectroscopy. The results of the research show that the as-prepared Ag_2S nanorods are monodispersed with sizes about 40 nm in diameter and 220 nm in length, and exhibit a high degree of crystallinity and good photoluminescence. Furthermore, an interesting mechanism is discussed for the formation of the Ag_2S nanorods.

Introduction

The reliance of future technologies on exploring facile and economic methods for the fabrication of one-dimensional (1D) systems has spurred intense and rapid development in the field of material synthesis. In particular, metal and semiconductor nanorods, as a family of 1D nanostructures, have been extensively pursued for their potential in building blocks for self-assembled nanoscale electronic circuits and energy-conversion devices. The highly ordered assembly of such nanorods is not only necessary for making functional devices, but also presents an opportunity to develop novel collective properties.[1] Various methods have been developed for the fabrication of the highly ordered 1D nanostructures.[2] Self-assembled CdS nanorods were prepared by an evaporation−condensation method at high temperature;[2a] copper oxide nanorods were prepared by a solid−liquid arc discharge process;[2b] and copper sulfide nanorods were synthesized by using the spin-coated monolayer of arachidic acid as molecular templates.[1a] Recently, biological factors have been exploited as synthesis directors for nanoparticles and nanofibers, because they could regulate the unique shapes and the exact sizes of various nanocrystals. The directed syntheses of semiconducting nanowires (ZnS and CdS), for example, were reported onto a virus-based scaffold.[3] In addition, this kind of biological surface modification of semiconductor and metal nanoparticles with antibodies, peptides, and protein is bioactive and biocompatible, which could provide bioactive functionalities throughout the nanocrystal surface for further biological interactions or couplings and then be used in life sciences for luminescence tagging, drug delivery, and many other aspects.[4]

As a semiconductor with a direct band gap of ∼1.0 eV at room temperature and relatively high absorption coefficient (10^4 $M^{-1}\cdot cm^{-1}$), monoclinic α-Ag_2S has a variety of potential applications, such as in photoconductors, photovoltaic cells, near-IR photon detectors, and solar-selective coating.[5] Many efforts have been focused on the synthesis of Ag_2S nanoparticles to enhance its performance in currently existing applications in photography and luminescent devices.[6] However, there were few reports concerning 1D Ag_2S nanomaterials. Very recently, silver sulfide nanowire arrays have been synthesized by the template of anodic aluminum oxide (AAO) membrane and by a gas−solid reaction approach. Zhao et al. created the self-supported pattern of Ag_2S nanorod arrays by a solution-growth method.[7]

BSA is the most studied protein, and it has a strong affinity to a variety of inorganic molecules binding to different sites, which makes possible utilization of BSA-decorated nanomaterials in a variety of supramolecular assemblies.[8] In this paper, we report a facile, controllable synthesis of semiconductor Ag_2S nanorods in the BSA aqueous solution at room temperature. These nanorods with round ends are monodispersed with sizes of about 40 nm in diameter and 220 nm in length. Microstructural analyses reveal that the highly ordered silver sulfide nanorods coated with BSA are single-crystalline in a monoclinic structure; this material also exhibits good photoluminescence. Furthermore, a rational mechanism based on coordination nucleation and the Ostwald ripening is proposed for the nanorod formation.

Experimental Section

Fabrication of the Ag_2S Nanorods. In a typical process, 50 mL of 50 mM silver nitrate (≥99.8%, M_w = 169.87 A.R.) aqueous solution and 100 mL of 1 mg/mL BSA (purity ≥98%, M_w = 68 000, Xiamen Sanland Chemicals Company Limited, China) aqueous solution were mixed with vigorous stirring at room temperature. The mixed solution of the BSA-Ag^+ emulsion was kept static under nitrogen protection for 6 h. Then 50 mL of 50 mM TAA (≥99.0%, M_w = 75.13) aqueous solution was added. Immediately after TAA addition, the solution changed to black, indicating the formation of colloidal Ag_2S

* To whom correspondence should be addressed. Phone: +86-373-3328117. Fax: +86-373-3328507. E-mail: yanglin1819@163.com (L. Yang), xingenjoy@163.com (R. Xing), and renqsh@sjtu.edu.cn (Q. Ren).
† College of Chemistry and Environmental Science, Henan Normal University.
‡ Biomedical Engineering, Shanghai Jiao Tong University.
§ Institute for Laser Medicine and Bio-Photonics, Shanghai Jiao Tong University.

10.1021/jp055603h CCC: $33.50
Published on Web 05/06/2006

particles. The mixed reaction solution was again kept static under ambient conditions for 72 h and then separated by high-speed centrifuging at 15 000 rpm. The collected black solid-state product was washed with double distilled water and ethanol three times and dried in a vacuum at room temperature for 24 h.

To investigate the influence of BSA on the formation of Ag_2S nanorods, two sets of control experiments were carried out as follows. Control A was to grow silver sulfide in the aqueous solution without BSA; control B was to vary the chelating time (mixing time) between Ag^+ and BSA. Each control experiment was done in the same conditions and procedure as the typical experiment.

Characterization. X-ray powder diffraction (XRD) measurements were performed on a Bruker D&Advance X-ray powder diffractometer with graphite monochromatized Cu Kα (λ = 0.15406 nm). A scanning rate of 0.05 deg/s was applied to record the pattern in the 2θ range of 20−70°. Scanning electron microscopy (SEM) images were taken on a JSM-5600LV scanning electron microscope equipped with an X-ray energy-dispersive spectroscopy (EDS) at an accelerating voltage of 20 kV. Transmission electron microscopy (TEM), accompanied by selected-area electron diffraction (SAED), was carried out on a JEOL JEM 100CX-II transmission electron microscope; high-resolution TEM (HRTEM) images were taken on a JEOL JEM-2010 transmission electron microscope. To prepare the TEM and HRTEM samples, a 5-μL droplet of dilute alcohol solution was dripped onto a carbon-coated copper grid, then dried at room temperature. The thermogravimetry−differential thermal analyses (TG-DTA) were performed on an EXSTAR TG/DTA6300 instrument. The ultraviolet−visible (UV−vis) absorption spectrum was recorded on a Perkin-Elmer Lambda 17 UV−visible spectrophotometer. A Shimadzu RF-540 PC instrument was used to record the photoluminescence (PL) spectrum. The FT-IR spectra were recorded on a Bio-Rad FTS-40 Fourier transform infrared spectrograph in the wavenumber range of 4000−400 cm^{-1}. The spectra were collected at 2 cm^{-1} resolution with 128 scans by preparing KBr pellets with a 3:100 "sample-to-KBr" ratio. Circular dichroism (CD) spectra (190−250 nm) were recorded on a Jasco J-810 spectropolarimeter. The same samples were repeated three times. This instrument had been calibrated previously for wavelength with benzene vapor, and for optical rotation with d_{10}-camphorsulfonic acid. A cell with a path length of 0.1 cm was used. The parameters used were as follows: bandwidth, 1 nm; step resolution, 0.1 nm; scan speed, 50 nm/min; response time, 0.25 s. Each spectrum was obtained after an average of six scans. Quantitative estimations of the secondary-structure content were made with the CDPro software package, which includes the programs CDSSTR, CONTIN, and SELCON3 (http://lamar.colostate.edu/~sreeram/CDPro/).[9] We used these three programs to analyze our CD spectra. The α-helical fractions extracted from the CDPro programs are in good agreement with those calculated based on empirical methods with ellipticities at either 208 or 222 nm.[10]

Results and Discussion

Characterization of the As-Prepared Ag_2S Nanorods. The synthesis of silver sulfide nanorods was performed by a two-step procedure. The first step was the generation of the silver(I)−BSA complex by mixing of the $AgNO_3$ and BSA solutions. The second step was the formation of Ag_2S nanorods by adding TAA into the above mixing solution at ambient temperature. TAA was comparatively unstable and slowly hydrolyzed to release S^{2-} ions into the reaction solution. We once tried to use Na_2S instead of TAA, but nanorods could not be formed, indicating that the slow release of sulfide ions was essential for the formation of the nanorods.

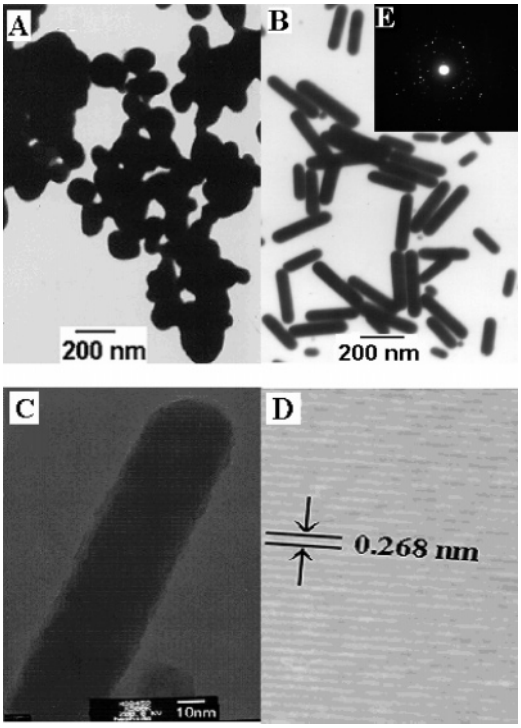

Figure 1. Low-magnification TEM image of Ag_2S (A) in the aqueous solution without BSA, (B) in the BSA aqueous solution from the typical experiment, (C) individual nanorod, (D) HRTEM image, and (E) SAED pattern in an area including many Ag_2S nanorods.

To investigate the influence of BSA on the formation of the Ag_2S nanorods, we carried out two sets of control experiments. Control A was done in the absence of BSA (see Figure 1A), in which the Ag_2S crystals were badly aggregated with elliptical particles. The result showed that the presence of BSA was a key factor in controlling and regulating the shape and size of the Ag_2S crystals. To further study the details about the effect of BSA, control B was done in the same conditions described as the typical experiment, apart from the chelating time between BSA and Ag^+. It was found that the appropriate chelating time (6 h) between BSA and Ag^+ was of great importance to achieve desirable results.

Figure 1B is a representative TEM image of the as-prepared Ag_2S nanorods in the BSA aqueous solution from the typical experiment. It can be seen that these nanorods are obviously well dispersed. Shown in Figure 1C is a TEM image recorded on an individual nanorod. The edges of the nanorod look fuzzy and amorphous, which could possibly be the BSA molecules. On the basis of this result, it can be hypothesized that the nanorods were coated with the BSA protein. The HRTEM image in Figure 1D provides further insight into its structure. It is observed that the nanorod exhibits good crystalline and clear lattice fringes. The experimental lattice fringe spacing, 0.268 nm, is consistent with the unique 0.2664 nm separation between two (120) planes in bulk acanthite Ag_2S crystallites. Figure 1E (inset of Figure 1B) is the corresponding SAED pattern, revealing that the nanorods are crystalline and can be indexed to monoclinic α-Ag_2S. Figure 2 presents the histogram of the nanorods, showing a relatively broad spread in length. A statistical analysis yields an average size of 40 nm in diameter and 220 nm in length and a size distribution standard deviation of 2.5 and 35 nm, respectively.

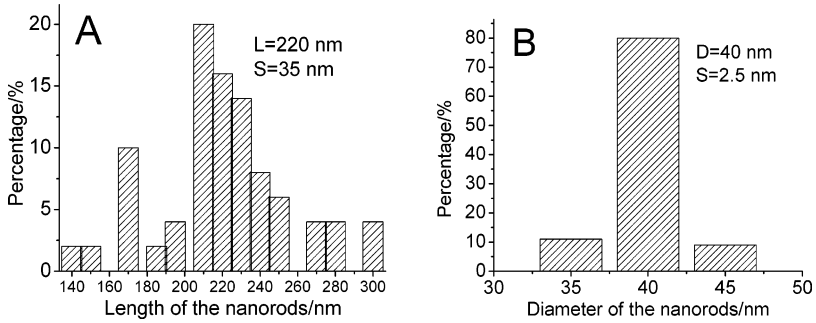

Figure 2. Histograms of the length (A) and the diameter (B) of the nanorods.

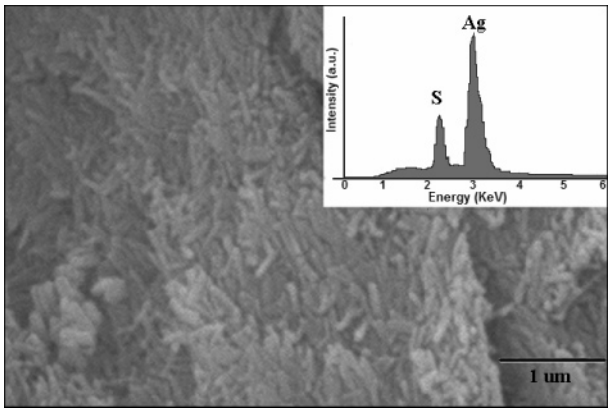

Figure 3. A representative SEM image of Ag_2S nanorods obtained from the typical experiment. Inset: The EDS pattern in an area including many Ag_2S nanorods.

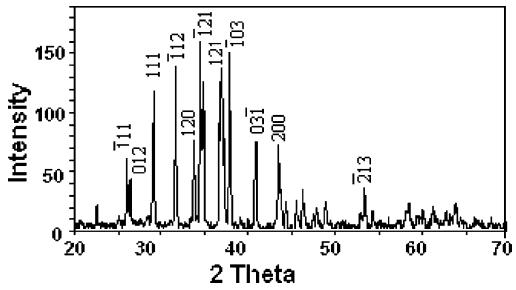

Figure 4. XRD pattern of the as-prepared Ag_2S nanorods.

Figure 3 shows a typical SEM image of the product obtained from the typical experiment. It can be seen that the product presents a rodlike morphology with nanometer-sized diameters and regular arrays. The SEM result is consistent with that obtained from TEM observation and further confirms the formation of the Ag_2S nanorods. The EDS spectrum (inset of Figure 3) of the Ag_2S nanorods shows the significant presence of only Ag and S with an atomic ratio (Ag/S) of nearly 2, in good agreement with the stoichiometric molar ratio of silver sulfide.

Figure 4 presents the XRD pattern of the as-prepared Ag_2S nanorods. In Figure 4, all peaks can be indexed to the monoclinic Ag_2S phase, in good agreement with the reported data for α-Ag_2S (JCPDS Card File 14-0072) after considering Scherrer broadening, which further confirmed the SAED result.

TG and DTA curves of pure BSA and the as-prepared nanorods were determined under air atmosphere at a heating rate of 10 deg/min from 50 to 800 °C. For the TG curve of pure BSA, there are two stages of weight loss. The first stage is from 180 to 480 °C, probably due to the escape of several kinds of small molecules, resulting from the intramolecular disintegration of the BSA molecules; the second stage is from 480 to 570 °C, owing to the combustion of the residues. Figure

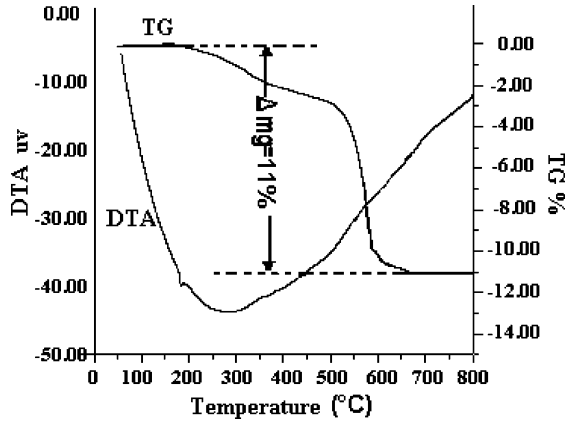

Figure 5. TG-DTA curves for the as-prepared Ag_2S nanorods.

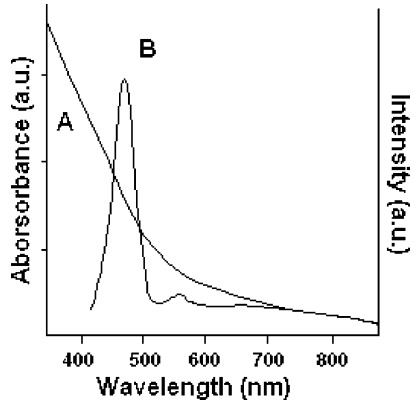

Figure 6. (a) UV−vis absorption spectrum and (b) PL spectrum of the resulting solution of the as-prepared Ag_2S nanorods. Excitation was performed at 378 nm.

5 illustrates the TG and DTA curves of the as-prepared nanorods obtained from the typical experiment. From the TG curve of the nanorods, it is observed that the first stage is from 200 to 510 °C and the second stage from 510 to 650 °C; the total weight loss is about 11% from 200 to 650 °C. Comparing the TG curve of the as-prepared nanorods with that of pure BSA, they have similar weight loss curves, except for the lag of the BSA breakup temperature. The enhancement of the thermal stability of BSA might be due to the interaction between BSA and Ag_2S nanocrystals. From the DTA curve of the nanorods, there is a wide endothermic peak from 50 to 650 °C, due to the transformation from α-Ag_2S to β-Ag_2S at 178 °C and the breakup and combustion of BSA molecules. According to the TEM results of the fuzzy periphery and high degree of crystallinity of the nanorod, it could be presumed that the protein (11%) be conjugated on the surface of the nanorods.

Figure 6 shows the UV−vis absorption and PL spectra of the product. The UV−vis absorption spectrum of the resulting

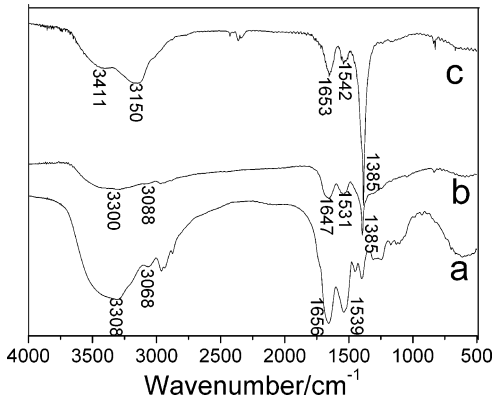

Figure 7. The FT-IR spectra of (a) pure BSA, (b) BSA-Ag^+, and (c) BSA-Ag_2S nanorods.

TABLE 1: The Main Peaks of Pure BSA, BSA-Ag^+, and BSA-Ag_2S from the IR Spectra

assignment	−OH (cm^{-1})	amide A′ (cm^{-1})	amide I (cm^{-1})	amide II (cm^{-1})	NO_3^- (cm^{-1})
Pure BSA	3308	3068	1656	1539	
BSA-Ag^+	3300	3088	1647	1531	1385
BSA-Ag_2S	3411	3150	1653	1542	1385

solution of the as-prepared Ag_2S nanorods is a rather featureless curve with gradually increasing absorbance toward shorter wavelengths (see Figure 6a) in accord with the results in the literature. This phenomenon is likely due to the overlap of absorption bands, which occur at different energies for nanocrystals having disparate sizes.[4c,11] The PL spectrum of the nanorods was obtained with the excitation wavelength of 378 nm (see Figure 6b). It exhibits a narrow emission peak centered at about 474 nm.[12] The relatively narrow fwhm with the value of 30 nm indicates that the sample is well disperse in the solution with few electronic defect sites.[13]

In addition, the influence of the reaction conditions on the Ag_2S nanorods growth has been systematically studied. First, we investigated the influence of the BSA concentration on the appearance of the nanorods. It was found that it was suitable for the growth and formation of the nanorods when the BSA concentration was 1−2 mg/mL. At a lower BSA concentration (0.5 mg/mL), there were mostly spherical silver sulfide nanoparticles and a few rods in appearance, while the high BSA concentration (4 mg/mL) did not lead to a detectable appearance change of the nanorods. Next, the silver ion concentration also affected distinctly the shape of nanorods. At a high silver ion concentration ($\geq$75 mM), Ag_2S nuclei tended to form coarse larger nanorods, whereas at a low silver ion concentration, uniform nanorods with regular shape can be obtained. Furthermore, the presence/absence of nitrogen protection also influenced the rod homogeneity. Without nitrogen protection, there were a wide range of nanorods from 80 to 300 in length; with nitrogen protection, the obtained products were uniform in rod size and morphology. To make a comparison, we also carried out the experiment with mild electromagnetic stirring instead of the static method throughout the aging process, and more nanoparticles and fewer short nanorods were obtained at last.

Formation Mechanism of the Ag_2S Nanorods. To study the formation mechanism of the Ag_2S nanorods in the BSA aqueous solution, the FT-IR spectra of pure BSA, BSA-Ag^+, and BSA-Ag_2S solutions were determined. The FT-IR spectra and the data of the main peaks are presented in Figure 7 and Table 1, respectively. The IR peaks of pure BSA at 3308, 3068, 1656, and 1539 cm^{-1} are assigned to the stretching vibration of −OH, amide A′ (mainly −NH stretching vibration), amide I, and amide II bands, respectively. The strong peak at ~1385 cm^{-1} in the BSA-Ag^+ and BSA-Ag_2S spectra is assigned to the absorption of nitrate ions, which was introduced by the addition of silver nitrate. Comparing the IR spectrum of BSA-Ag^+ with that of pure BSA, there are negligible variations in the characteristic peaks of −OH groups, amide I, and amide II bands, but the characteristic peak of amide A′ bands shifted to a high wavenumber of about 20 cm^{-1}, suggesting that there might be coordination interaction between silver ions and N−H groups of BSA, which played an important role in the formation of Ag_2S nanoparticles. Comparing the IR spectrum of BSA-Ag_2S with that of pure BSA, the characteristic peaks of −OH groups and amide A′ bands shifted to a high wavenumber of about 100 and 80 cm^{-1}, respectively. The results showed that there might be the conjugate bonds between the Ag_2S nanorod surfaces and −OH and −NH groups in BSA.[14] In addition, the BSA protein also involves 17 disulfide bonds with one free thiol in cysteine residues, which might also be attracted to the Ag_2S nanorods for surface binding via thiolate linkages. Results in the literature have also shown that the thiol-containing amino acids were proved to be excellent nucleating agents for the synthesis of metal sulfide nanoparticles.[4c,15] Therefore, it can be concluded that these binding interactions (coordination for BSA and Ag^+ and conjugate for BSA and Ag_2S nanorods) are probably responsible for the resulting BSA-Ag_2S nanorods formation.

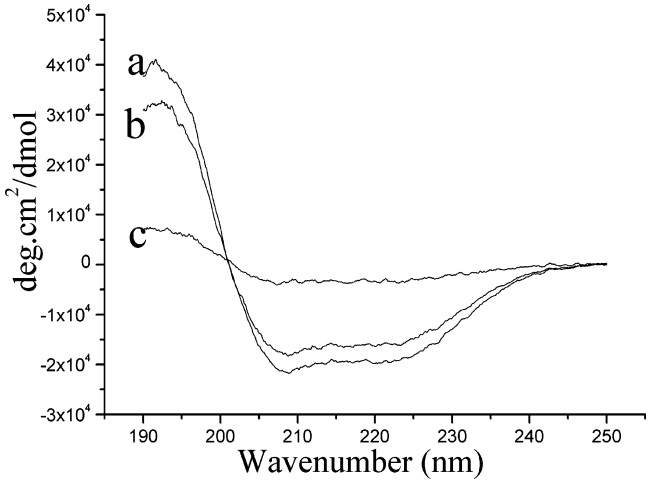

Figure 8. The CD spectra of (a) pure BSA, (b) BSA-Ag^+, and (c) BSA-Ag_2S nanorod solutions.

To further study the formation mechanism of the nanorods in the BSA aqueous solution, changes of the secondary structures of BSA in the system were determined by using CD spectroscopy, which is a valuable spectroscopic technique for studying protein and its complex.[16] The CD spectra of pure BSA, BSA-Ag^+, and BSA-Ag_2S solutions are given in Figure 8 when the mean residue concentration of BSA is 1.6×10^{-6} mol/L. From Figure 8, it can be seen that the CD curve of the BSA-Ag^+ solution is similar to that of the pure BSA solution, while the CD spectrum of the BSA-Ag_2S solution is different from that of pure BSA. The experimental data of the system are presented in Table 2 and RMSD means the error between the experiments and conversion CD spectra. From Table 2, pure BSA contains 60.9% α-helices and 4.4% β-sheets, in good agreement with the previous reports.[17] Comparing the CD results of BSA-Ag^+ and BSA-Ag_2S with those of pure BSA, the content of α-helices of BSA decreased 9.5% and 51.7% and the β-sheet content increased 4.2% and 31.9%, respectively, whereas the content of turns and random coils did not change much. There are 3.6 amino acid residues in every ring of the α-helix segment. It is

TABLE 2: The Percentages of the Secondary Structures of Pure BSA, BSA-Ag^+, and BSA-Ag_2S at 298 K and pH 5.5

assignment	α-helix/%	β-sheet/%	turn/%	random/%	RMSD
pure BSA	60.9	4.4	12.5	22.3	10.1
BSA-Ag^+	51.4	8.6	15.3	24.7	9.1
BSA-Ag_2S	9.2	36.3	22.5	32.0	8.5

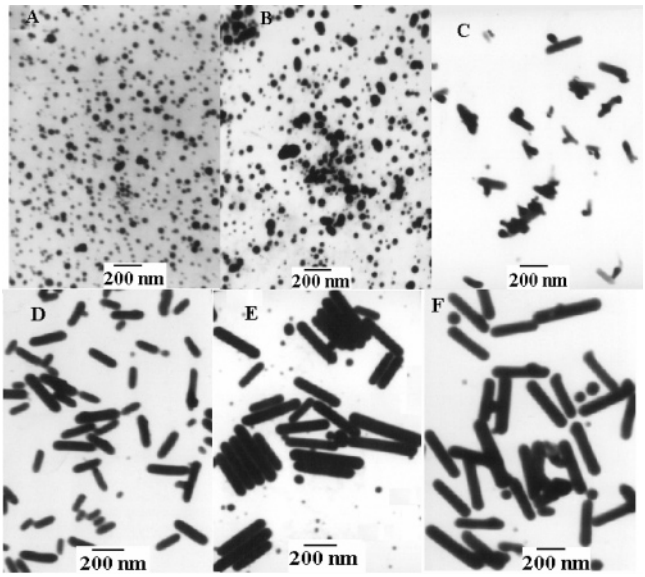

Figure 9. TEM images of Ag_2S nanorods obtained after different aging time in the typical experiment: (A) 12, (B) 24, (C) 36, (D) 60, (E) 72, and (F) 96 h, respectively.

well-known that the hydrogen bond formed between the oxygen atom of the (*i*) carboxylic group and the hydrogen atom of the ($i + 4$) amino group is a key stable factor to keep the α-helix structure of the protein. And the β-sheet structure can be seen as a kind of special α-helix only with two amino acid residues through stretching, resulting from the break of the hydrogen bond.[18] According to the experimental data above, it can be seen that silver ions only induced the smaller deformation of the BSA molecules in the BSA-Ag^+ solution, whereas there were bigger changes of the BSA conformation in the BSA-Ag_2S nanorod solution, resulting from the strong conjugate bonds between BSA and surfaces of the colloidal nanorods. From the changes of the α-helix and β-sheet content, it can be presumed that α-helices might be stretched and transformed into β-sheets, owing to the impairment or break of hydrogen bonds.

TEM analyses were performed on the solutions after aging for different periods to keep track of the nanorod growth. Figure 9A−F displays the typical morphology of the products by aging for 12, 24, 36, 60, 72, and 96 h, respectively. After 12 h of aging, its TEM image (Figure 9A) shows that the sample was composed of monodisperse nanoparticles with diameters in the range of 10−20 nm. Twenty-four hours later, the nanoparticles grew larger and short rods appeared (Figure 9B). At an aging time of 36 h, there were mainly short nanorods with nanoparticles attached (Figure 9C). When aged for 60 h, these nanorods had a wide range in length and all nanoparticles disappeared (Figure 9D). If the aging time was further increased to 72 h, these nanorods grew homogeneously up to about 220 nm in length (Figure 9E). To investigate further, the aging time was even prolonged to 96 h; however, it was found that the nanorod length was almost unchanged (Figure 9F). According to the above phenomena, it could be presumed that the nanorods are growing at the expense of the colloidal particles in the Ostwald ripening process.

According to the discussion above, it is proposed that the highly ordered Ag_2S nanorods could be formed through the coordination nucleation and Ostwald ripening process. After the silver nitrate solution was added into the BSA aqueous solution, silver ions coordinated with some groups (such as −NH and −SH) of BSA, resulting in the relatively high silver ion concentration around these groups. Then TAA was added and the slow-released S^{2-} ions combined with the Ag^+ ions to form Ag_2S nuclei on some special sites of BSA. Once the nuclei were formed, the growth of Ag_2S nanoparticles started on them. Then the colloidal Ag_2S particles gradually transformed into nanorods, followed by a dissolution−precipitation equilibration in the Ostwald ripening process. As a result, the as-prepared nanorods were obtained.

Conclusions

To sum up, the highly ordered Ag_2S nanorods conjugated with BSA were successfully achieved by sequentially adding $AgNO_3$ and TAA into the BSA aqueous solution. It exhibits a high degree of crystallinity and good photoluminescence. A rational mechanism based on coordination nucleation and the Ostwald ripening process is proposed for the formation of the Ag_2S nanorods. This synthetic process is very simple, clean, controllable, and reproducible. The exploitation of a common protein to prepare the protein-conjugated nanorods provides a novel pathway for biomodified nanomaterials, which could be promising in life sciences for luminescence tagging, drug delivery, and implantable microdevices, as well as for molecular electronics.

Acknowledgment. This study was supported by the National Basic Research Program of China (Grant No. 2005CB724306) and the National Science Foundation of China (Grant No. 20371016). We are grateful to the Lab for Special Functional Materials of Henan University for the help with HRTEM measurements. We also thank the referees for helpful comments.

References and Notes

(1) (a) Mao, G. Z.; Dong, W. F.; Kurth, D. G.; Mohwald, H. *Nano Lett.* **2004**, *4*, 249. (b) Huang, Y.; Duan, X. F.; Cui, Y.; Lauhon, L. J.; Kim, K.; Lieber, C. M. *Science* **2001**, *294*, 1313. (c) de Picciotto, R.; Stormer, H. L.; Pfeiffer, L. N.; Baldwin, K. W.; West, K. W. *Nature* **2001**, *411*, 51.

(2) (a) Dong, L. F.; Gushtyuk, T.; Jiao, J. *J. Phys. Chem. B.* **2004**, *108*, 1617. (b) Yao, W. T.; Yu, S. H.; Zhou, Y.; Jiang, J.; Wu, Q. S.; Zhang, L.; Jiang, J. *J. Phys. Chem. B* **2005**, *109*, 14011.

(3) Mao, C. B.; Solis, D. J.; Reiss, B. D.; Kottmann, S. T.; Sweeney, R. Y.; Hayhurst, A.; Georgiou, G.; Iverson, B.; Belcher, A. M. *Science* **2004**, *303*, 213.

(4) (a) Cha, J. N.; Stucky, G. D.; Morse, D. E.; Deming, T. J. *Nature* **2000**, *403*, 289. (b) Hartgerink, J. D.; Beniash, E.; Stupp, S. I. *Science* **2001**, *294*, 1684. (c) Meziani, M. J.; Sun, Y. P. *J. Am. Chem. Soc.* **2003**, *125*, 8015. (d) Reches, M.; Gazit, E. *Science* **2003**, *300*, 625.

(5) (a) *Numerical Data and Functional Relationships in Science and Technology*, *Group 3*, *Crystal and Solid State Physics*, *17e*, *Semiconductors: Physics of Non-Tetrahedrally Bonded Elements and Binary Compounds I*; Madelung, O., Ed.; Springer-Verlag: Berlin, 1983; p 157. (b) Hodes, G.; Manassen, J.; Cahen, D. *Nature* **1976**, *261*, 403. (c) Abass, A. K. *Solar Energy Mater.* **1988**, *17*, 375.

(6) (a) Mitchell, J. W. J. *Imaging Sci. Technol.* **1998**, *42*, 215. (b) Baetzold, R. C. J. *Imaging Sci. Technol.* **1999**, *43*, 375. (c) Bruhwiler, D.; Leiggener, C.; Glaus, S.; Calzaferri, G. *J. Phys. Chem. B* **2002**, *106*, 3770.

(7) (a) Peng, X. S.; Meng, G. W.; Zhang, J.; Wang, X. F.; Zhao, L. X.; Wang, Y. W.; Zhang, L. D. *Mater. Res. Bull.* **2002**, *37*, 1369. (b) Wen, X. G.; Wang, S. H.; Xie, Y. T.; Li, X. Y.; Yang, S. H. *J. Phys. Chem. B* **2005**, *109*, 10100. (c) Lu, Q. Y.; Gao, F.; Zhao, D. Y. *Angew. Chem., Int. Ed.* **2002**, *41*, 1932.

(8) Mamedova, N. N.; Kotov, N. A.; Rogach, A. L.; Studer, J. *Nano Lett.* **2001**, *1*, 281.

(9) Sreerama, N.; Woody, R. W. *Anal. Biochem.* **2000**, *287*, 253.

(10) (a) Wu, C. S. C.; Ikeda, K.; Yang, J. T. *Biochemistry* **1981**, *20*, 566. (b) Chen, Y. H.; Yang, J. T.; Chau, K. H. *Biochemistry* **1974**, *13*, 3350.

(11) (a) Pileni, M. P.; Motte, L.; Billoudet, F.; Mahrt, J.; Willig, F. *Mater. Lett.* **1997**, *31*, 255. (b) Schaaff, T. G.; Rodinone, A. J. *J. Phys. Chem. B* **2003**, *107*, 10416. (c) Brelle, M. C.; Zhang, J. Z.; Nguyen, L.; Mehra, R. K. *J. Phys. Chem. A* **1999**, *103*, 10194.

(12) (a) Brühwiler, D.; Leiggener, C.; Glaus, S.; Calzaferri, G. *J. Phys. Chem. B* **2002**, *106*, 3770. (b) Leiggener, C.; Brühwiler, D.; Calzaferri, G. *J. Mater. Chem.* **2003**, *13*, 1969. (c) Brühwiler, D.; Seifert, R.; Calzaferri, G. *J. Phys. Chem. B* **1999**, *103*, 6397.

(13) Nie, W.; An, L. J.; Jiang, B. Z.; Ji, X. L. *Chem. Lett.* **2004**, *33*, 836.

(14) (a) Leff, D. V.; Brandt, L.; Heath, J. R. *Langmuir* **1996**, *12*, 4723. (b) Keating, C. D.; Kovaleski, K. M.; Natan, M. J. *J. Phys. Chem. B* **1998**, *102*, 9404. (c) Keating, C. D.; Kovaleski, K. K.; Natan, M. J. *J. Phys. Chem. B* **1998**, *102*, 9414.

(15) (a) Foster, J. F. In *Albumin Structure, Function and Uses*; Rosenoer, V. M., Oratz, M., Rothschild, M. A., Eds.; Pergamon: Oxford, U.K., 1977; p 53. (b) Sasaki, Y. C.; Yasuda, K.; Suzuki, Y.; Ishibashi, T.; Satoh, I.; Fujiki, Y.; Ishiwata, S. *Biophys. J.* **1997**, *72*, 1842. (c) Bae, W.; Mehra, R. K. *J. Inorg. Biochem.* **1998**, *70*, 125

(16) (a) Blauer, G.; Harmatz, D. *Biochim. Biophys. Acta* **1972**, *278*, 89. (b) Trull, F. R.; Ibars, O.; Lightner, D. A. *Arch. Biochem. Biophys.* **1992**, *298*, 710. (c) Blauer, G.; Harmatz, D.; Snir, J. *Biochim. Biophys. Acta* **1972**, *278*, 68.

(17) (a) Reed, R. G.; Feldhoff, R. C.; Clute, O.; Peterson, T., Jr. *Biochemistry* **1975**, *14*, 4578. (b) Williams, R. W.; Dunker, A. K. *J. Mol. Biol.* **1981**, *152*, 783. (c) Gelamo, E. L.; Silva, C. H. T. P.; Imasato, H.; Tabak, M. *Biochim. Biophys. Acta* **2002**, *1594*, 84.

(18) (a) Yang, L.; Guo, Y. M.; Ma, X. M.; Hu, Z. G.; Zhu, S. F.; Zhang, X. Y.; Jiang, K. *J. Inorg. Biochem.* **2003**, *93*, 197. (b) Yang, L.; Shen, Q. M.; Zhou, J. G.; Jiang, K. *Mater. Lett.* **2005**, *59*, 2889.